iScience

Article

Hydrogel bead-based isothermal detection (BEAD-ID) for assessing the activity of DNA-modifying enzymes

Graphical abstract

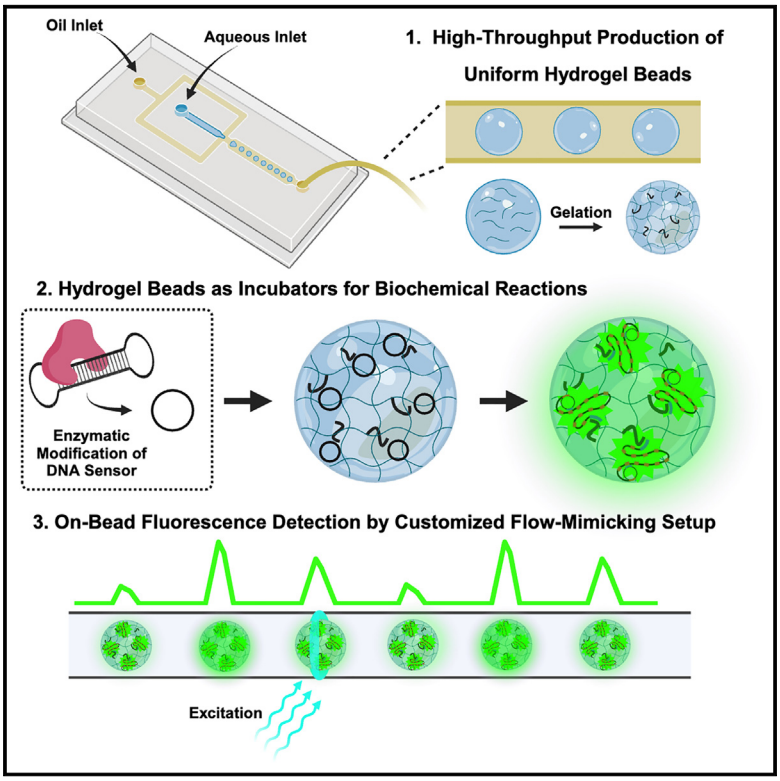

Authors

Kathrine Nygaard Borg, Ayush Shetty, Guangyao Cheng, ..., Birgitta Ruth Knudsen, Cinzia Tesauro, Yi-Ping Ho

Correspondence

ypho@cuhk.edu.hk

In brief

Sensor; Fluidics; Nanotechnology; Methodology in biological sciences

Highlights

- BEAD-ID enables on-bead detection of DNA-modifying enzyme activity
- Hydrogel beads capture and amplify enzyme-modified nanosensors effectively
- Platform shows sensitivity to TOP1 and EcoRI activity in varied matrices
- High-throughput detection setup quantifies enzyme activity at 352 Hz efficiently

Borg et al., 2024, iScience *27*, 111332
December 20, 2024
https://doi.org/10.1016/j.isci.2024.111332

CellPress

iScience

CellPress
OPEN ACCESS

Article

Hydrogel bead-based isothermal detection (BEAD-ID) for assessing the activity of DNA-modifying enzymes

Kathrine Nygaard Borg,[1] Ayush Shetty,[1] Guangyao Cheng,[1] Shaodi Zhu,[1] Tianle Wang,[1] Wu Yuan,[1] Ho Pui Ho,[1] Birgitta Ruth Knudsen,[2] Cinzia Tesauro,[2] and Yi-Ping Ho[1,3,4,5,6,*]

[1]Department of Biomedical Engineering, The Chinese University of Hong Kong, Shatin, Hong Kong SAR 00000, China
[2]Department of Molecular Biology and Genetics, Aarhus University, 8000 Aarhus C, Denmark
[3]Centre for Biomaterials, The Chinese University of Hong Kong, Hong Kong SAR, China
[4]Hong Kong Branch of CAS Center for Excellence in Animal Evolution and Genetics, Hong Kong SAR, China
[5]State Key Laboratory of Marine Pollution, City University of Hong Kong, Hong Kong SAR, China
[6]Lead contact
*Correspondence: ypho@cuhk.edu.hk
https://doi.org/10.1016/j.isci.2024.111332

SUMMARY

DNA-modifying enzymes are crucial in biological processes and have significant clinical implications. Traditional quantification methods often overlook enzymatic activity, the true determinants of enzymes' functions. We present hydrogel Bead-based Isothermal Detection (BEAD-ID), utilizing uniform hydrogel bead-based microreactors to evaluate DNA-modifying enzyme activity on-bead. We fabricated homogeneous oligo-conjugated polyacrylamide (oligo-PAA) beads *via* droplet microfluidics, optimized for capturing and amplifying enzyme-modified nanosensors. By incorporating DNA oligos within the hydrogel network, BEAD-ID retains isothermally amplified products, facilitating *in situ* detection of enzyme activities on-bead. We validate BEAD-ID by quantifying human topoisomerase I (TOP1) and restriction endonuclease EcoRI, showing a direct correlation between enzyme concentration and fluorescence intensity, demonstrating the platform's sensitivity (6.25 nM TOP1, 6.25 U/μL EcoRI) and reliability in food matrix (25 U/μL EcoRI). Additionally, a customized flow cytometry-mimicking setup allows high-throughput detection at 352 Hz with objective assessment. BEAD-ID, offering flexibility and scalability, is a promising tool for studying DNA-modifying enzymes.

INTRODUCTION

DNA-modifying enzymes are essential enzymes involved in fundamental processes including DNA replication, repair, recombination, and gene expression. In clinical practice, the activities of DNA-modifying enzymes may serve as a biomarker, as well as drug targets. One prominent example is human topoisomerase I (TOP1), which plays a vital role in resolving topological stress generated during DNA transcription, and replication or recombination by introducing transient single-stranded breaks followed by rotation of the cleaved DNA strand around the non-cleaved strand.[1] Upon cleavage, TOP1 remains covalently attached to the 3′-end of the DNA and is released by religation of the nick. Camptothecin (CPT), a mother compound of commonly employed anticancer drug derivatives,[2–4] selectively inhibits the TOP1 re-ligation step by binding to the transient single-stranded cleavage complex (TOP1cc). The drug-induced TOP1cc leads to cell death due to the formation of double-stranded DNA breaks upon collision with the transcription or replication machinery.[5] Restriction endonucleases (REs), also a class of DNA-modifying enzymes ubiquitously expressed in bacteria, serve to protect the host against invading viruses by cleaving viral DNA at specific base sequences, known as the restriction sites.[6,7] REs are therefore extensively utilized in applications including PCR, gene mapping, and cloning, taking the feature of specific binding and cleavage of a given RE on the restriction sites. Technologies including western blotting and quantitative reverse transcription-PCR (qRT-PCR) are widely employed for the quantification of targeted DNA-modifying enzymes, however, assessment of the enzymatic activities, the true determinants of enzymes' biological functions, remains challenging. The activity of enzymes may be altered by the post-translational modifications, suggesting that the mRNA levels or protein amounts and the enzyme activity may not always align,[8] as validated by techniques including cleavage-ligation assays for TOP1 activity, or gel electrophoresis and fluorescence resonance energy transfer (FRET) for assessing the digestion activity of REs.[9–11] While recent advancements have enhanced the analytical sensitivity in enzyme detection by exploiting fast turnover rates of substrate-to-product conversions, many reported biosensors are either limited in sensitivity or demand costly and time-consuming processes.[12] Stougaard

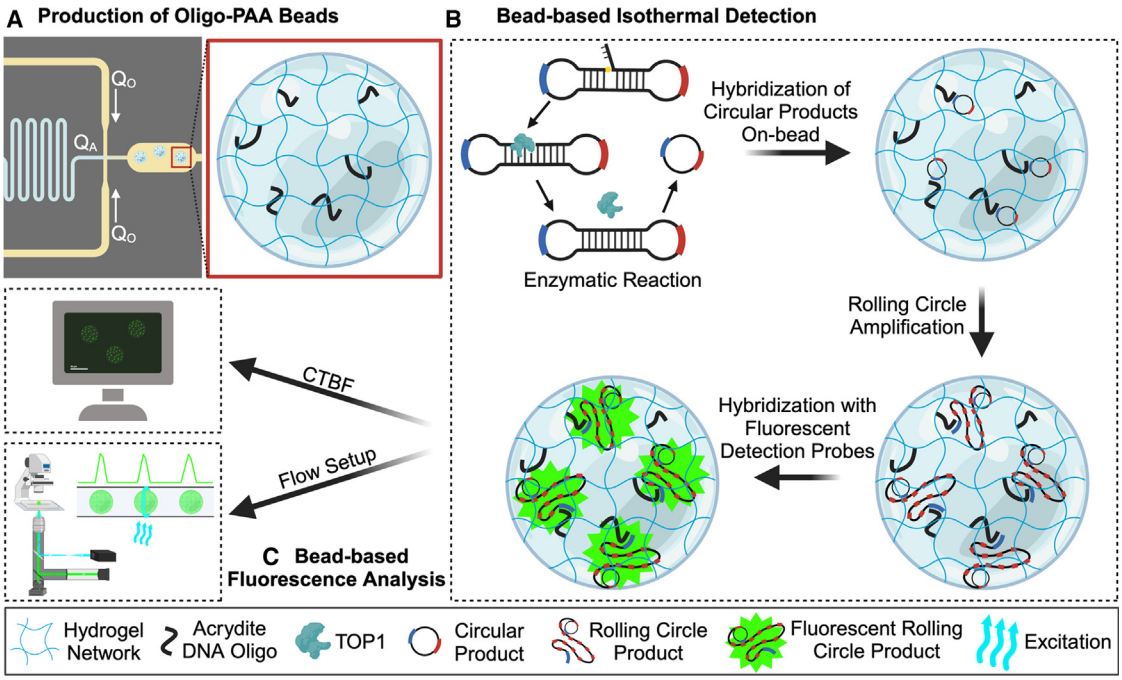

Figure 1. Hydrogel Bead-based Isothermal Detection (BEAD-ID)

(A) Droplet microfluidics is employed to generate uniform hydrogel beads crosslinked with DNA oligos, serving as capturing agents of circular products and as primers for the rolling circle amplification (RCA).

(B) BEAD-ID initiates with the circularization of DNA nanosensors containing sequences recognized by the targeted DNA-modifying enzymes. The resulting circular products hybridize with the DNA oligos within the hydrogel network, acting as templates for the ensuing RCA using the same DNA oligos as primers. The resulting amplified products are identified by complementary fluorescent detection probes, facilitating the fluorescent detection of the hydrogel beads through (c) standard image analysis using corrected total bead fluorescence (CTBF) assessment or a customized flow cytometry-mimicking platform (the illustration is created with BioRender.com).

et al.[13] employ on-slide anchored isothermal amplification for the facile detection of enzyme activity of DNA-modifying enzymes, termed Rolling circle Enhanced Enzyme Activity Detection (REEAD), taking advantage of rolling circle amplification (RCA) to boost up the signal produced from DNA cleavage-ligation events. REEAD has proven a robust and reliable measure of enzyme activity at the single molecule level, even with the sample of crude cell extracts.[14–16] REEAD has been validated for detecting the activity of various targets, including TOP1 from human cells and fruit flies,[17,18] Flp- and Cre recombinases,[19] and most recently, bacterial REs.[20] Compared to existing enzyme activity detection assays, REEAD achieves high sensitivity (10 amol/μL) owing to the catalytic properties of DNA-modifying enzymes.[13] However, the original format of REEAD relies on massive acquisition and analysis of images through fluorescence microscopy, potentially posing a limitation for further promotion of enzymatic activities as a biomarker in the clinical setting.[12,21] Recent efforts have therefore focused on revising the readout formats to for example fluorescence scanner,[22] chemiluminescence,[23] and colorimetric detection,[24] While these revisions may simplify the process of data acquisition, the assay remains on a solid surface, i.e., functionalized slides or strips supplied by specific vendors. Also, compared to fluorescence microscopy detection, the sensitivity of these simplified readouts is limited to around nmol/μL for the detection of TOP1.[22]

Hydrogel beads have gained widespread popularity for biochemical applications, such as diagnostics and drug delivery, given the capabilities of automation together with integrated analysis,[25–27] the features of hydrophilicity, biocompatibility, and tunable properties.[28,29] Unlike solid and impermeable particles, hydrogel beads are highly porous and therefore permeable, providing an expanded surface-to-volume ratio conducive to versatile functionalization. For instance, hydrogel beads have been instrumental in incorporating detection probes or targeting ligands crucial for biochemical reactions.[30] By tuning the ratio of crosslinkers and polymerization catalysts, the hydrogel porosity may be tailored for cell or biomolecule entrapment, DNA barcoding, display of proteins, and utilization as nanoreactors for enzymatic reactions.[31–34] Last but not least, recent advancements in microfluidics have enabled a high-throughput production of uniform hydrogel beads (>1,000 beads per second) at an affordable price.[35]

Herein, BEAD-ID (hydrogel Bead-based Isothermal Detection) is developed as an integrated, and yet highly customizable, platform for the assessment of enzymatic activities on-bead. Polyacrylamide (PAA) gels were chosen as a model to validate the proposed BEAD-ID workflow for the characteristics of chemically inert, transparency in the visible spectra, wide accessibility, and validated chemistry for oligo functionalization.[31] As depicted in Figure 1, uniform and oligo-functionalized PAA hydrogel

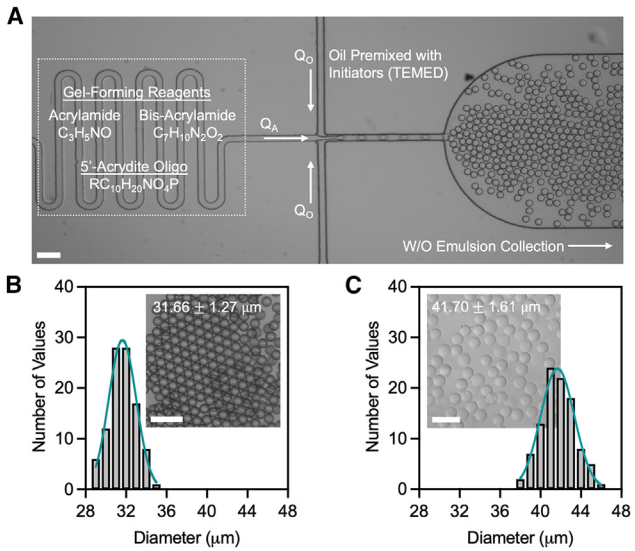

Figure 2. Production of oligo-conjugated polyacrylamide beads

(A) Design of the flow-focusing droplet generator for the production of water-in-oil (W/O) emulsions at flow rates of 2 μL/min and 8 μL/min for aqueous (Q_A) and the continuous oil (Q_O) phases, respectively.

(B) Size distribution (n = 100) and a representative brightfield image of the produced W/O emulsions.

(C) Size distribution (n = 100) and a representative brightfield image of the released oligo-PAA beads. Histograms are fitted with Gaussian distribution. Scalebars: 100 μm.

(oligo-PAA) beads, as a micro-bioreactor, are firstly produced by droplet microfluidics. The functionalized oligos serve dual purposes of capturing the enzymatically modified nanosensors and priming the RCA reactions, thereby retaining the RCA amplified products on-bead. Followed by recognition of the fluorescent detection probes, the amplified products, indicative of the level of enzyme activities, are then quantified either by image analysis or with a customized flow cytometry-mimicking setup. The platform is validated by the detection and quantification of TOP1 activity (sensitivity at 6.25 nM) and RE activity from EcoRI (sensitivity at 6.25 U/μL in optimized buffer, and 25 U/μL in milk matrix). BEAD-ID has shown promise for an analysis of up to 7,000 beads per experiment under the customized flow setup. Taken together, BEAD-ID is expected to serve as a new analytic platform for the investigation of enzymatic activities in a high-throughput and objective manner.

RESULTS

Characterization of homogeneous oligo-conjugated polyacrylamide beads

Water-in-oil (W/O) emulsions encapsulating the acrylamide monomers, 5′-acrydite oligos, and crosslinkers were produced by a droplet generator as illustrated in Figure 2A.[36] The size of W/O emulsions was tuned by alternating the volumetric flow rates of the dispersed aqueous (Q_A) and the continuous oil (Q_O) phase.[35] Under the optimized flow ratio (Q_O/Q_A = 4), the resulting W/O emulsions were measured 31.66 ± 1.27 μm in diameter (Figure 2B), a size range suitable for biochemical reactions.[37]

Following overnight polymerization, oligos were functionalized in the crosslinked PAA network. The oligo-PAA beads were measured 41.70 ± 1.61 μm (CV = 3.9%) in diameter after the release from the oil phase (Figure 2C). The level of swelling was optimized to allow sufficient solute diffusion of biological reactants such as ions, DNA circular products, and polymerases, across the microporous network.[38] The DNA oligos functionalized within the hydrogel network were characterized to be approximately 10 μM per bead (1.15×10^8 DNA oligos/bead), yielding an incorporation efficiency of 50–60%, in line with earlier observations (see Figure S1).[32,39,40] FAM-labelled reporter probes, complementary to the DNA oligo within the hydrogel mesh, were introduced to further verify DNA oligo functionalization and to investigate the relationship between fluorescence signal and bound fluorescent probes (Figure 3A). Various amounts of reporter probes, relative to those in the oligo-PAA beads, were tested. As depicted in Figure 3B, fluorescence intensity was observed consistently increased as the reporter probe amount rose from 0.375× to 5× (equivalent to 60 amol/bead to 960 amol/bead). This concentration range of reporter probe was applied according to the minimally detectable and saturated signal under the intended settings by a fluorescence microscope. Note that the signal was observed indistinguishable from the background noise and over-saturated for probe concentrations lower than 60 amol/bead and higher than 960 amol/bead, respectively (see Figure S2A). As shown in Figure 3C, and in Figure S2B, corrected total bead fluorescence (CTBF) was used as a quantitative indicator of fluorescence intensity on beads, as defined by McCloy et al.[41] This result confirmed that the acrydite DNA oligos were functionalized within the hydrogel network and the measured fluorescence may serve as a measure of enzymatic activities with BEAD-ID.

Assessment of enzymatic activities via BEAD-ID by fluorescent microscopy

Two model DNA-modifying enzymes, TOP1 and EcoRI, were subsequently introduced for the assessment of BEAD-ID by fluorescent microscopy. As shown in Figure 4A, TOP1 may recognize, cleave, and re-ligate a motif on the open double-looped dumbbell DNA nanosensor, designed based on a TOP1-specific DNA sequence.[13] The TOP1 DNA nanosensor also contains a sequence (blue loop) complementary to the recognition site on the oligos conjugated on-bead. After RCA, FAM-labelled detection probes, complementary to the amplified red loop sequence of TOP1 DNA nanosensor, are introduced for fluorescence readout. DNA circular products produced by titrated amounts (50, 25, 12.5, 6.25, and 0 nM) of purified TOP1 enzyme were introduced in the BEAD-ID assay. As observed in Figure 4B and quantified by CTBF in Figure 4C (see Figure S3), the fluorescent signals exhibited a positive correlation with the quantity of TOP1. When 50 nM of heat-inactivated purified TOP1 was presented, a fluorescent signal was not observed, verifying that the designed TOP1 DNA nanosensor measured the enzymatic activities, instead of the enzyme quantity *per se* (Figure S4).

Analogous to the TOP1 sensing scheme, EcoRI activity was assessed by the DNA nanosensor as illustrated in Figure 5A. The EcoRI nanosensor is composed of two DNA hairpins each with a double-stranded stem containing the restriction

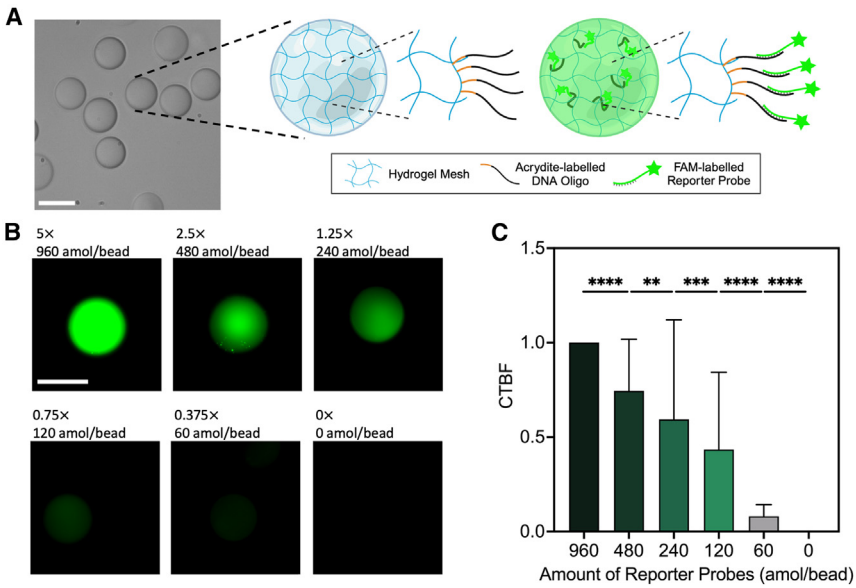

Figure 3. Characterization of fluorescent signal on-bead by fluorescence microscopy

(A) Schematic of acrydite DNA oligos conjugation into the hydrogel mesh and hybridization of the complementary fluorescent reporter probes (illustration created with BioRender.com).

(B) Visualization of the reporter probes hybridized to oligo-PAA beads (amount shown as the total number of reporter probes available per oligo-PAA bead (amol/bead)) during 1-h incubation at 37°C.

(C) CTBF quantification of the fluorescent intensity measured after incubation of an identical number of oligo-PAA beads with reporter probes in the range of 0–960 amol per bead. The presented data are from three independent experiments (n = 3) with standard deviation calculated between the mean fluorescence intensity of each replicate. Each experiment includes 10-image Z-stacks of at least 10 oligo-PAA beads. Statistical analysis was performed using non-parametric Kruskal-Wallis test followed by Dunn's multiple comparison test (**p < 0.0021, ***p < 0.0002, ****p < 0.0001). Scalebars: 50 μm.

site specific to EcoRI.[20] Upon cleavage by EcoRI, the two sticky ends, complementary to each other, may hybridize and produce a dumbbell structure with a nick. T4 DNA ligase was subsequently introduced to ligate the nick, producing a closed circular product. The red loop and blue loop, indicating the primer site and readout site, serve for hybridizing the circular product with the oligo-PAA beads and capturing the fluorescent detection probes, respectively. Under optimal buffer, the fluorescence was observed to decrease according to the titrated dilution of EcoRI (Figure 5B). The measured CTBF further validated that the fluorescent signals measured across different concentrations were significantly different (Figure 5C, see Figure S5A). Given the potential of using EcoRI activity for the detection of foodborne pathogens, we further explored the capability of BEAD-ID in a milk matrix. Despite the signal-to-noise (S/N) ratio being compromised in the milk matrix (Figure 5D), CTBF remained valid for the quantification of EcoRI activities in the range of 0.25–0.5 U/μL (Figure 5E, see Figure S5B). Collectively, these results highlight the adaptability of BEAD-ID to assess the activities of DNA-modifying enzymes in limited quantities.

Quantification of fluorescence using microfluidic flow setup

Subsequently, a tailored microfluidic flow setup (Figure 6A), designed for high-throughput detection of fluorescent oligo-PAA beads akin to flow cytometry, was established as an objective

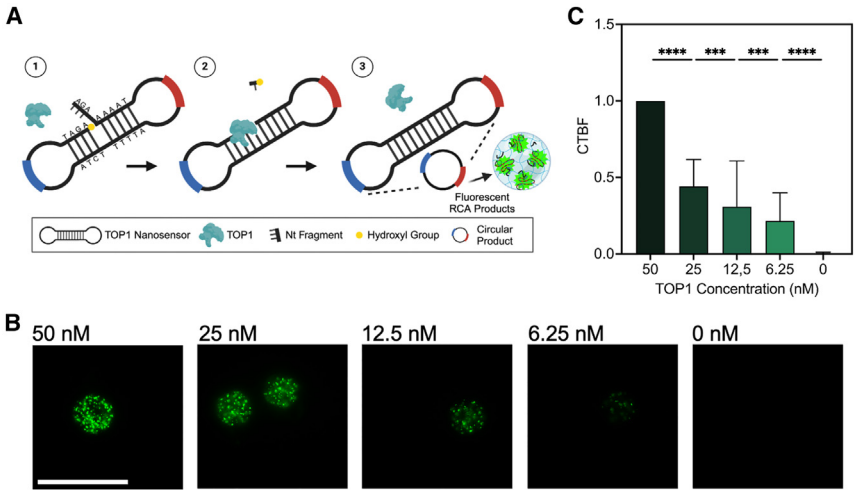

Figure 4. Assessment of topoisomerase I activity via BEAD-ID by fluorescent microscopy

(A) The DNA nanosensor designed for the measurement of TOP1 activity contains a TOP1-specific recognition site, where the arrow points toward the cleavage site. The single-stranded DNA nanosensor may self-fold into a double-looped structure with a nick. Upon recognition, cleavage, and religation by TOP1, a circular product is produced. The red loop and blue loop illustrate the primer site, complementary to the oligos on-bead, and the readout site, complementary to the fluorescent detection probes, respectively (illustration created with BioRender.com).

(B) Visualization of fluorescent rolling circle products on-beads obtained by BEAD-ID using 0.1 μM DNA nanosensors modified by titrated concentrations of purified TOP1 enzyme (50-0 nM), following the procedure described in the 'hydrogel bead-based isothermal detection (BEAD-ID)' in the STAR Methods section. Scalebar: 100 μm.

(C) CTBF quantification of BEAD-ID results. Data are presented as the mean ± standard deviation calculated between the mean fluorescence intensity from three independent experiments (n = 3). Each experiment includes 10-image Z-stacks of at least 10 oligo-PAA beads. Statistical analysis was performed using non-parametric Kruskal-Wallis test followed by Dunn's multiple comparison test (***p < 0.0006, ****p < 0.0001).

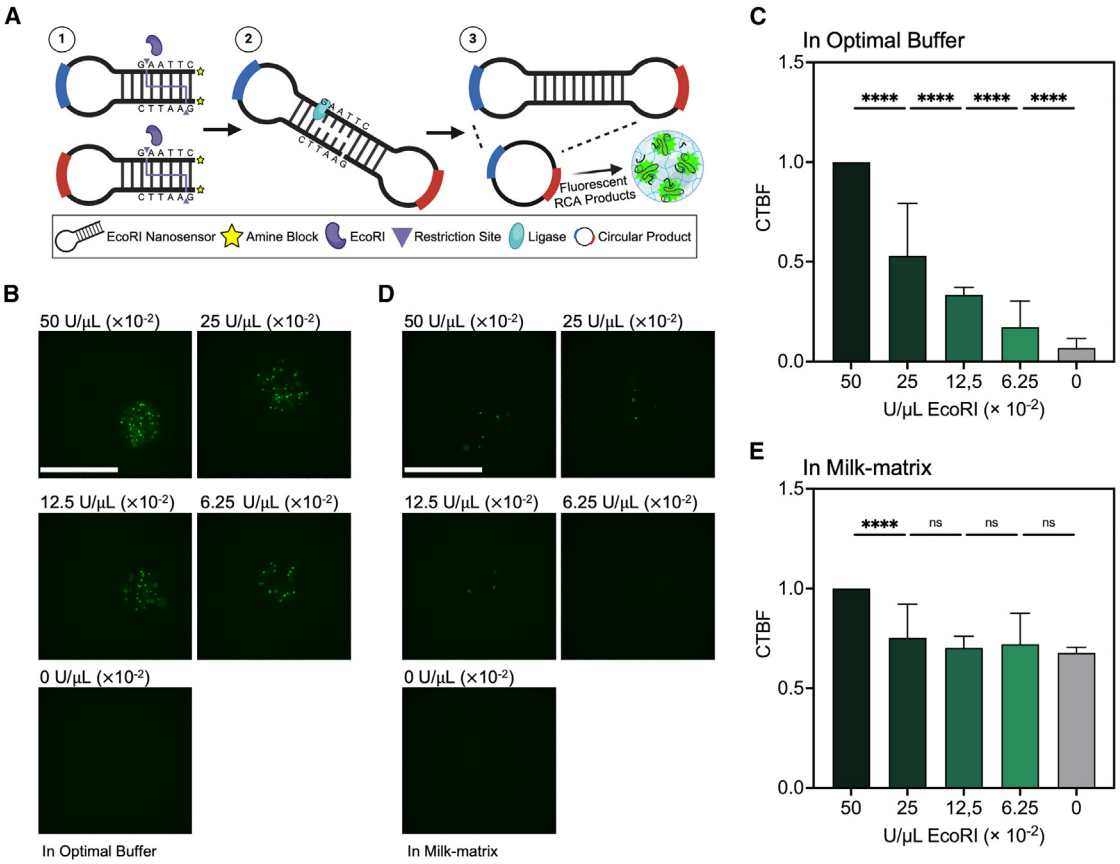

Figure 5. Assessment of EcoRI activity via BEAD-ID by fluorescent microscopy

(A) The DNA nanosensor designed for the measurement of EcoRI activity is composed of two hairpin structures each with an EcoRI-specific restriction site. Upon cleavage by EcoRI, the two sticky ends complementary to each other are ligated by T4 ligase, forming a circular structure as the template for RCA on-bead (illustration is created with BioRender.com).

(B) Fluorescent images and (C) CTBF quantification of fluorescence on-bead of BEAD-ID amplified DNA nanosensors (1 μM of each) obtained using titrated concentrations of EcoRI enzyme up to 0.5 U/μL in optimal buffer.

(D) Fluorescent images and (E) CTBF quantification of fluorescence on-bead for the beads subjected to DNA nanosensors (1 μM of each) modified by titrated concentrations of EcoRI enzyme up to 0.5 U/μL in milk-matrix. Data are plotted as the mean ± standard deviation calculated from the mean fluorescence intensities from three independent experiments (n = 3). Each experiment includes 10-image Z-stacks of at least 10 oligo-PAA beads. Statistical analysis was performed using non-parametric Kruskal-Wallis test followed by Dunn's multiple comparison test (****p < 0.0001, ns = nonsignificant). Scalebars: 100 μm.

and automatic assessment platform. Briefly, hydrogel beads were introduced into a microchannel in a flow rate of 10 μL/min (equivalent to 352 Hz) controlled by a syringe pump. Upon appropriate excitation of FAM, the emitted photons were measured by a photomultiplier tube (PMT). A customized post-analysis module constructed by LabVIEW and Python (see Figure S6) was used for the characterization of fluorescence intensities measured per bead. Parameters including peak height, area under the curve (AUC), and peak width (Figure 6B) were acquired according to previous studies.[39] Quantification of peak height, as shown in Figure 6C, suggests a monotonic correlation between the measured fluorescence and the concentration of reporter probe, corroborated with the CTBF quantification. As a model enzyme, the activity of TOP1 on-bead was assessed by the microfluidic flow setup. A similar correlation of fluorescence signal and enzyme concentration was also observed in Figure 6D. Note that up to 7,000 beads were assessed in the flow system per experiment, ensuring the statistical power and thereby providing an objective analysis compared to CTBF quantification. Representative histograms shown in Figure S7 approximating a normal distribution further validate that the sample size assessed by the flow setup may be considered sufficiently large.

DISCUSSION

Traditional methods investigating DNA-modifying enzymes often assess the quantity *per* se, instead of enzymatic activities, a decisive factor of their biological functions. A previously established REEAD assay demonstrates high sensitivity on the assessment of enzymatic activities (10 amol/μL for TOP1) through innovatively deploying the catalytic properties of DNA-modifying enzymes, however, the time-consuming process of image acquisition and analysis via fluorescence microscopy limits its applicability in

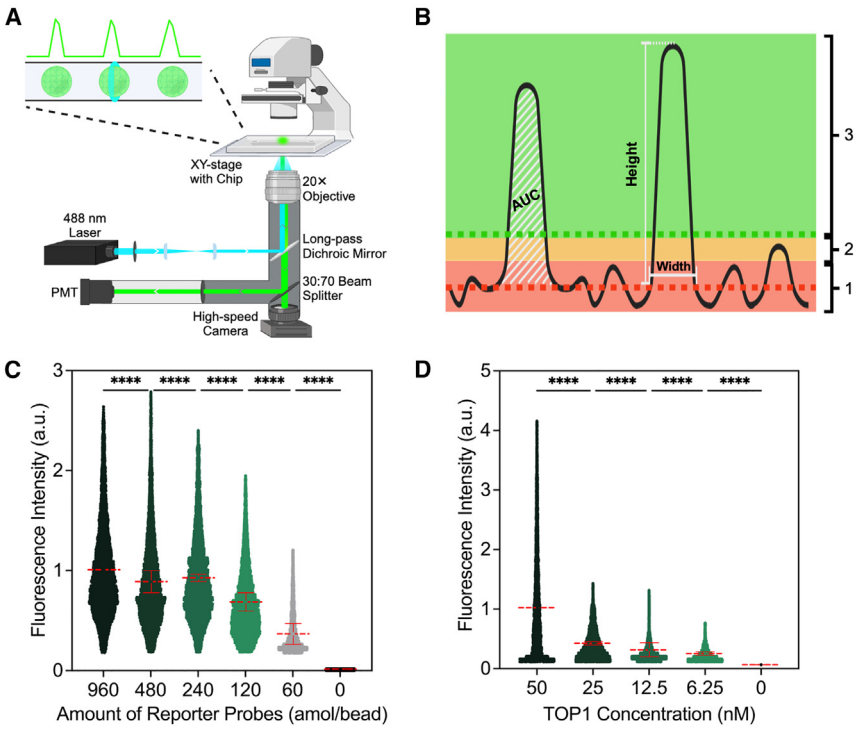

Figure 6. Quantification of fluorescence by a customized microfluidic flow setup

(A) Schematic of the customized detection module. Briefly, fluorescence beads within a flow microchannel are excited by a 488 nm laser diode. The emitted fluorescence is collected through an objective and guided via a dichroic mirror to a beam splitter which then directs 70% of the light to a high-speed camera and 30% to a photomultiplier tube.

(B) Definition of peak parameters and detection thresholds. 1: mean of the noise from negative (blank) samples (red dashed line) and standard deviation zone (red), 2: zone of maximum noise measured from blank samples (yellow). 3: zone above threshold for peak detection (green). Area under the curve (AUC) is the integrated area from peak base (baseline obtained from blank samples) to the apex of the peak. Height of the peak is calculated from the base to the apex of the peak. Width of the peak is calculated at the widest part of the peak, occurring at the base of the peak.

(C) Peak height quantification of fluorescence on-beads displaying reporter probe (960-0 amol per bead) from a minimum of 5,727 peaks per reporter probe concentration.

(D) Peak height quantification of TOP1 activity displayed on-beads via BEAD-ID using TOP1-modified DNA nanosensor (0.1 μM). For each TOP1 concentration (50-0 nM) a minimum of 4,237 peaks were applied in the analysis. Data plotted as scatterplot showing mean ± standard deviation calculated from three independent experiments (n = 3) after normalization to the mean of the highest concentration. Statistical analysis was performed using one-way ANOVA test followed by Tukey's multiple comparison test (****p < 0.0001).

point-of-care testing. To address these challenges, we developed BEAD-ID, a platform designed to enhance flexibility and scalability in enzyme activity assessment. BEAD-ID incorporates a bead-based microreactor, which confines the biochemical reactions and integrates the workflow on-bead. As measured by the CTBF, BEAD-ID has demonstrated high sensitivity, comparable to previous surface-based REEAD results.[22–24] However, a large variation from the CTBF analysis has been observed, most likely ascribed to the relatively small sample sizes, limited by the image-based analysis, as reflected in the calculated S/N ratios of 192, 21, and 6 for TOP1 and EcoRI in optimal buffers and EcoRI in food matrix, respectively. Additionally, the dataset acquired from CTBF is not normally distributed, as verified against the normality tests of Shapiro-Wilk, another indicator that the sample size may be a limiting factor. Integration of a customized flow cytometry-mimicking platform has therefore been introduced to increase the throughput, and has shown improved S/N ratios of 427 for the reporter probe and 240 for TOP1, providing significantly larger datasets with reduced variation. The incorporation of this customized optical detection platform allows a collection of sufficient amount and normally distributed datasets, and enable the extraction of minimum detectable concentrations, as exampled in Figure 6 for the reporter probe signal and the TOP1 enzyme activity. Determined by the widely employed 3σ approach,[42] where limit-of-detection (LOD) is defined as the blank mean plus three times the standard deviation of the blank sample. The LOD was estimated to be 0.99 amol/bead for the reporter probe and 0.72 nM for TOP1. Overall, the improved S/N ratios and LOD indicate robust and reliable fluorescence-based detection of enzyme activity with the customized optical flow system. Together with the previous verifications on the specificities of DNA nanosensors designed for the activities of Flp and Cre recombinases,[14] TOP1 from *Mycobacterium smegmatis*[43] and *Plasmodium* species,[15] and EcoRI,[20] we anticipate that BEAD-ID will be immediately applicable in foodborne pathogen detection or a wide range of biochemical applications, featured in high-throughput, objective assessment, and tailorable properties of the hydrogel beads.

Limitations of the study

The size and porosity of PAA microgel beads, as well as the oligo functionalization protocols, used in this study have been optimized to accommodate isothermal amplification by Phi29 DNA polymerase with the designed DNA nanosensors. However, the parameters reported may not be universally applicable, given that the polymerases, macromolecules, and various lengths of oligos may vary in size and charges in different buffers under different pH or contain various additives. To extend the applicability of the BEAD-ID setup to widespread biochemical reactions, fine-tuning of beads size, porosity, and/or materials may be necessary. With this said, a set of generalizable design rules is anticipated to promote BEAD-ID for applications beyond the assessment of DNA-modifying enzymes' activities.

RESOURCE AVAILABILITY

Lead contact

Further information and requests for resources and reagents should be directed to and will be fulfilled by the lead contact, Y.-P.H. (ypho@cuhk.edu.hk).

Materials availability

This study did not generate new unique reagents.

Data and code availability

- Data: data reported in this paper will be shared by the lead contact upon request.
- Code: all original code is available in this paper's supplemental information.
- Any additional information required to reanalyze the data reported in this paper is available from the lead contact upon request.

ACKNOWLEDGMENTS

The authors would like to express their gratitude the support received by the Research Grants Council of Hong Kong Special Administrative Region, China (project #: CUHK 14207121, 14219922 and C5005-23WF), the VC Discretionary Fund provided by the Chinese University of Hong Kong, Hong Kong Special Administrative Region, China (project #: 8601014) and the State Key Laboratory in Marine Pollution (SKLMP), the City University of Hong Kong, Hong Kong Special Administrative Region, China, under the scheme of Seed Collaborative Research Fund (project #: SKLMP/SCRF/0042).

AUTHOR CONTRIBUTIONS

Conceptualization, K.N.B., W.Y., H.P.H., C.T., B.R.K., and Y.-P.H.; methodology, K.N.B., A.S., G.C., S.Z., and T.W.; formal analysis, K.N.B.; writing – original draft preparation, K.N.B. and Y.-P.H.; writing – review and editing, K.N.B., A.S., G.C., S.Z., T.W., W.Y., H.P.H., C.T., B.R.K., and Y.-P.H.; supervision, Y.-P.H.

DECLARATION OF INTERESTS

The authors declare that they have no known competing financial interests or personal relationships that could have appeared to influence the work reported in this paper.

STAR★METHODS

Detailed methods are provided in the online version of this paper and include the following:

- KEY RESOURCES TABLE
- EXPERIMENTAL MODEL AND STUDY PARTICIPANT DETAILS
- METHOD DETAILS
  - DNA oligonucleotides
  - Microfluidic chip designs and fabrication
  - Fabrication of oligo-conjugated polyacrylamide beads
  - Hydrogel bead-based isothermal detection (BEAD-ID)
  - Hybridization of reporter probes to oligo-PAA beads and microscopic observations
- QUANTIFICATION OF OLIGOS IN OLIGO-PAA BEADS
  - Setup of the microfluidic flow setup
  - Data processing by LabVIEW and Python
- QUANTIFICATION AND STATISTICAL ANALYSIS

SUPPLEMENTAL INFORMATION

Supplemental information can be found online at https://doi.org/10.1016/j.isci.2024.111332.

Received: June 20, 2024
Revised: September 25, 2024
Accepted: November 4, 2024
Published: November 6, 2024

REFERENCES

1. Staker, B.L., Hjerrild, K., Feese, M.D., Behnke, C.A., Burgin, A.B., Jr., and Stewart, L. (2002). The mechanism of topoisomerase I poisoning by a camptothecin analog. Proc. Natl. Acad. Sci. USA *99*, 15387–15392. https://doi.org/10.1073/pnas.242259599.
2. Pommier, Y. (2006). Topoisomerase I inhibitors: Camptothecins and beyond. Nat. Rev. Cancer *6*, 789–802. https://doi.org/10.1038/nrc1977.
3. Tesauro, C., Simonsen, A.K., Andersen, M.B., Petersen, K.W., Kristoffersen, E.L., Algreen, L., Hansen, N.Y., Andersen, A.B., Jakobsen, A.K., Stougaard, M., et al. (2019). Topoisomerase I activity and sensitivity to camptothecin in breast cancer-derived cells: a comparative study. BMC Cancer *19*, 1158. https://doi.org/10.1186/s12885-019-6371-0.
4. Tesauro, C., Keller, J.G., Gromova, I., Gromov, P., Frohlich, R., Erlandsen, J.U., Andersen, A.H., Stougaard, M., and Knudsen, B.R. (2020). Different Camptothecin Sensitivities in Subpopulations of Colon Cancer Cells Correlate with Expression of Different Phospho-Isoforms of Topoisomerase I with Different Activities. Cancers *12*, 1240. https://doi.org/10.3390/cancers12051240.
5. Pourquier, P., and Pommier, Y. (2001). Topoisomerase I-mediated DNA damage. Adv. Cancer Res. *80*, 189–216. https://doi.org/10.1016/s0065-230x(01)80016-6.
6. Roberts, R.J. (1976). Restriction endonucleases. CRC Crit. Rev. Biochem. *4*, 123–164. https://doi.org/10.3109/10409237609105456.
7. Kessler, C., Neumaier, P.S., and Wolf, W. (1985). Recognition sequences of restriction endonucleases and methylases–a review. Gene *33*, 1–102. https://doi.org/10.1016/0378-1119(85)90119-2.
8. Stougaard, M., and Ho, Y.P. (2014). DNA-based nanosensors for next-generation clinical diagnostics via detection of enzyme activity. Expert Rev. Mol. Diagn. *14*, 1–3. https://doi.org/10.1586/14737159.2014.863151.
9. Nitiss, J.L., Soans, E., Rogojina, A., Seth, A., and Mishina, M. (2012). Topoisomerase assays. Curr. Protoc. Pharmacol. *3*, 1–27. https://doi.org/10.1002/0471141755.ph0303s57.
10. Southern, E. (1979). Gel electrophoresis of restriction fragments. Methods Enzymol. *68*, 152–176. https://doi.org/10.1016/0076-6879(79)68011-4.
11. Ma, C., Tang, Z., Wang, K., Tan, W., Yang, X., Li, W., Li, Z., and Lv, X. (2007). Real-time monitoring of restriction endonuclease activity using molecular beacon. Anal. Biochem. *363*, 294–296. https://doi.org/10.1016/j.ab.2007.01.018.
12. Ma, F., Li, C.C., and Zhang, C.Y. (2021). Nucleic acid amplification-integrated single-molecule fluorescence imaging for in vitro and in vivo biosensing. Chem. Commun. *57*, 13415–13428. https://doi.org/10.1039/d1cc04799j.
13. Stougaard, M., Lohmann, J.S., Mancino, A., Celik, S., Andersen, F.F., Koch, J., and Knudsen, B.R. (2009). Single-molecule detection of human topoisomerase I cleavage-ligation activity. ACS Nano *3*, 223–233. https://doi.org/10.1021/nn800509b.
14. Andersen, F.F., Stougaard, M., Jørgensen, H.L., Bendsen, S., Juul, S., Hald, K., Andersen, A.H., Koch, J., and Knudsen, B.R. (2009). Multiplexed detection of site specific recombinase and DNA topoisomerase activities at the single molecule level. ACS Nano *3*, 4043–4054. https://doi.org/10.1021/nn9012912.
15. Juul, S., Nielsen, C.J.F., Labouriau, R., Roy, A., Tesauro, C., Jensen, P.W., Harmsen, C., Kristoffersen, E.L., Chiu, Y.L., Frøhlich, R., et al. (2012). Droplet microfluidics platform for highly sensitive and quantitative detection of malaria-causing Plasmodium parasites based on enzyme activity measurement. ACS Nano *6*, 10676–10683. https://doi.org/10.1021/nn3038594.
16. Hede, M.S., Fjelstrup, S., Lötsch, F., Zoleko, R.M., Klicpera, A., Groger, M., Mischlinger, J., Endame, L., Veletzky, L., Neher, R., et al. (2018). Detection of the Malaria causing Plasmodium Parasite in Saliva from Infected Patients using Topoisomerase I Activity as a Biomarker. Sci. Rep. *8*, 4122. https://doi.org/10.1038/s41598-018-22378-7.

17. Keller, J.G., Tesauro, C., Coletta, A., Graversen, A.D., Ho, Y.P., Kristensen, P., Stougaard, M., and Knudsen, B.R. (2017). On-slide detection of enzymatic activities in selected single cells. Nanoscale *9*, 13546–13553. https://doi.org/10.1039/c7nr05125e.

18. Juul-Kristensen, T., Keller, J.G., Borg, K.N., Hansen, N.Y., Foldager, A., Ladegaard, R., Ho, Y.-P., Loeschcke, V., and Knudsen, B.R. (2023). Topoisomerase 1 Activity Is Reduced in Response to Thermal Stress in Fruit Flies and in Human HeLa Cells. Biosensors *13*, 950. https://doi.org/10.3390/bios13110950.

19. Juul, S., Ho, Y.P., Stougaard, M., Koch, J., Andersen, F.F., Leong, K.W., and Knudsen, B.R. (2011). Microfluidics-mediated isothermal detection of enzyme activity at the single molecule level. Annu. Int. Conf. IEEE Eng. Med. Biol. Soc. *2011*, 3258–3261. https://doi.org/10.1109/IEMBS.2011.6090885.

20. Petersen, K.V., Tesauro, C., Hede, M.S., Pages, C., Marcussen, L.B., Keller, J.G., Bugge, M., Holm, K., Bjergbæk, L., Stougaard, M., et al. (2022). Rolling Circle Enhanced Detection of Specific Restriction Endonuclease Activities in Crude Cell Extracts. Sensors *22*, 7763. https://doi.org/10.3390/s22207763.

21. Sakamoto, S., Komatsu, T., Watanabe, R., Zhang, Y., Inoue, T., Kawaguchi, M., Nakagawa, H., Ueno, T., Okusaka, T., Honda, K., et al. (2020). Multiplexed single-molecule enzyme activity analysis for counting disease-related proteins in biological samples. Sci. Adv. *6*, eaay0888. https://doi.org/10.1126/sciadv.aay0888.

22. Keller, J.G., Mizielinski, K., Petersen, K.V., Stougaard, M., Knudsen, B.R., and Tesauro, C. (2022). Simple and Fast Rolling Circle Amplification-Based Detection of Topoisomerase 1 Activity in Crude Biological Samples. J. Vis. Exp. *190*, e64484. https://doi.org/10.3791/64484.

23. Keller, J.G., Petersen, K.V., Mizielinski, K., Thiesen, C., Bjergbæk, L., Reguera, R.M., Pérez-Pertejo, Y., Balaña-Fouce, R., Trejo, A., Masdeu, C., et al. (2023). Gel-Free Tools for Quick and Simple Screening of Anti-Topoisomerase 1 Compounds. Pharmaceuticals *16*, 657. https://doi.org/10.3390/ph16050657.

24. Keller, J.G., Petersen, K.V., Knudsen, B.R., and Tesauro, C. (2022). Simple and Fast DNA-Based Tool to Investigate Topoisomerase 1 Activity, a Biomarker for Drug Susceptibility in Colorectal Cancer. In Recent Understanding of Colorectal Cancer Treatment, K.-Y. Jeong, ed. (Intech Open), pp. 1–16. https://doi.org/10.5772/intechopen.105758.

25. Weber, T.A., Metzler, L., Fosso Tene, P.L., Brandstetter, T., and Rühe, J. (2022). Single-Color Barcoding for Multiplexed Hydrogel Bead-Based Immunoassays. ACS Appl. Mater. Interfaces *14*, 25147–25154. https://doi.org/10.1021/acsami.2c04361.

26. Alpsoy, L., Sedeky, A.S., Rehbein, U., Thedieck, K., Brandstetter, T., and Rühe, J. (2023). Particle ID: A Multiplexed Hydrogel Bead Platform for Biomedical Applications. ACS Appl. Mater. Interfaces *15*, 55346–55357. https://doi.org/10.1021/acsami.3c12122.

27. Wulandari, D.A., Tsuru, K., Minamihata, K., Wakabayashi, R., Goto, M., and Kamiya, N. (2024). A Functional Hydrogel Bead-Based High-Throughput Screening System for Mammalian Cells with Enhanced Secretion of Therapeutic Antibodies. ACS Biomater. Sci. Eng. *10*, 628–636. https://doi.org/10.1021/acsbiomaterials.3c01386.

28. Jung, I.Y., Kim, J.S., Choi, B.R., Lee, K., and Lee, H. (2017). Hydrogel Based Biosensors for In Vitro Diagnostics of Biochemicals, Proteins, and Genes. Adv. Healthcare Mater. *6*, 1601475. https://doi.org/10.1002/adhm.201601475.

29. Amiri, M., Khazaeli, P., Salehabadi, A., and Salavati-Niasari, M. (2021). Hydrogel beads-based nanocomposites in novel drug delivery platforms: Recent trends and developments. Adv. Colloid Interface Sci. *288*, 102316. https://doi.org/10.1016/j.cis.2020.102316.

30. Roh, Y.H., Lee, H.J., and Bong, K.W. (2019). Microfluidic Fabrication of Encoded Hydrogel Microparticles for Application in Multiplex Immunoassay. BioChip J. *13*, 64–81. https://doi.org/10.1007/s13206-019-3104-z.

31. Bibi, Z., Sattar, H., Asif Nawaz, M., Karim, A., Pervez, S., Ali Ul Qader, S., and Aman, A. (2022). Polyacrylamide hydrogel carrier (matrix-type macrogel beads): Improvement in the catalytic behavior, stability, and reusability of industrially valuable xylanase from a thermophile Geobacillus stearothermophilus. Curr. Res. Biotechnol. *4*, 229–237. https://doi.org/10.1016/j.crbiot.2022.03.006.

32. Wang, Y., Cao, T., Ko, J., Shen, Y., Zong, W., Sheng, K., Cao, W., Sun, S., Cai, L., Zhou, Y.L., et al. (2020). Dissolvable Polyacrylamide Beads for High-Throughput Droplet DNA Barcoding. Adv. Sci. *7*, 1903463. https://doi.org/10.1002/advs.201903463.

33. Fryer, T., Rogers, J.D., Mellor, C., Kohler, T.N., Minter, R., and Hollfelder, F. (2022). Gigavalent Display of Proteins on Monodisperse Polyacrylamide Hydrogels as a Versatile Modular Platform for Functional Assays and Protein Engineering. ACS Cent. Sci. *8*, 1182–1195. https://doi.org/10.1021/acscentsci.2c00576.

34. Rakszewska, A., Stolper, R.J., Kolasa, A.B., Piruska, A., and Huck, W.T.S. (2016). Quantitative Single-Cell mRNA Analysis in Hydrogel Beads. Angew. Chem., Int. Ed. Engl. *55*, 6698–6701. https://doi.org/10.1002/anie.201601969.

35. Wan, J., Bick, A., Sullivan, M., and Stone, H.A. (2008). Controllable microfluidic production of microbubbles in water-in-oil emulsions and the formation of porous microparticles. Adv. Mater. *20*, 3314–3318. https://doi.org/10.1002/adma.200800628.

36. Abate, A.R., Kutsovsky, M., Seiffert, S., Windbergs, M., Pinto, L.F.V., Rotem, A., Utada, A.S., and Weitz, D.A. (2011). Synthesis of monodisperse microparticles from non-Newtonian polymer solutions with microfluidic devices. Adv. Mater. *23*, 1757–1760. https://doi.org/10.1002/adma.201004275.

37. Wei, Y., Cheng, G., Ho, H.P., Ho, Y.P., and Yong, K.T. (2020). Thermodynamic perspectives on liquid-liquid droplet reactors for biochemical applications. Chem. Soc. Rev. *49*, 6555–6567. https://doi.org/10.1039/c9cs00541b.

38. Girardo, S., Träber, N., Wagner, K., Cojoc, G., Herold, C., Goswami, R., Schlüßler, R., Abuhattum, S., Taubenberger, A., Reichel, F., et al. (2018). Standardized microgel beads as elastic cell mechanical probes. J. Mater. Chem. B *6*, 6245–6261. https://doi.org/10.1039/c8tb01421c.

39. Borg, K.N., Cheng, G., Shetty, A., Wang, T., Tesauro, C., Knudsen, B.R., and Ho, Y.-P. (2023). An Integrated Platform for the Assessment of Fluorescent Signals in Hydrogel Beads Produced by Droplet Microfluidics. In 2023 IEEE 23rd International Conference on Nanotechnology (NANO) (IEEE), pp. 180–184.

40. Klein, A.M., Mazutis, L., Akartuna, I., Tallapragada, N., Veres, A., Li, V., Peshkin, L., Weitz, D.A., and Kirschner, M.W. (2015). Droplet barcoding for single-cell transcriptomics applied to embryonic stem cells. Cell *161*, 1187–1201. https://doi.org/10.1016/j.cell.2015.04.044.

41. McCloy, R.A., Rogers, S., Caldon, C.E., Lorca, T., Castro, A., and Burgess, A. (2014). Partial inhibition of Cdk1 in G 2 phase overrides the SAC and decouples mitotic events. Cell Cycle *13*, 1400–1412. https://doi.org/10.4161/cc.28401.

42. Armbruster, D.A., and Pry, T. (2008). Limit of blank, limit of detection and limit of quantitation. Clin. Biochem. Rev. *29*, S49–S52.

43. Franch, O., Han, X., Marcussen, L.B., Givskov, A., Andersen, M.B., Godbole, A.A., Harmsen, C., Nørskov-Lauritsen, N., Thomsen, J., Pedersen, F.S., et al. (2019). A new DNA sensor system for specific and quantitative detection of mycobacteria. Nanoscale *11*, 587–597. https://doi.org/10.1039/c8nr07850e.

44. Qin, D., Xia, Y., and Whitesides, G.M. (2010). Soft lithography for micro- and nanoscale patterning. Nat. Protoc. *5*, 491–502. https://doi.org/10.1038/nprot.2009.234.

45. Motulsky, H.J., and Brown, R.E. (2006). Detecting outliers when fitting data with nonlinear regression - a new method based on robust nonlinear regression and the false discovery rate. BMC Bioinf. *7*, 123. https://doi.org/10.1186/1471-2105-7-123.

STAR★METHODS

KEY RESOURCES TABLE

REAGENT or RESOURCE	SOURCE	IDENTIFIER
Chemicals, peptides, and recombinant proteins		
1H,1H,2H,2H-perfluoro-1-octanol	Sigma-Aldrich	Cat #370533
Acrylamide/BIS 30% (37.5:1)	Bio-Rad	Cat #1610158
Ammonium persulfate	Sigma-Aldrich	Cat #17874
Formamide	Thermo Fischer Scientific	Cat #17899
Glycerol	Beyotime Biotechnology	Cat #ST1353
HFE-7500 3M™ Novec™	Fluorochem	Cat #F051243
PBS pH 7.4 Gibco™	Thermo Fischer Scientific	Cat #10010023
Pico-Surf® (5% in Novec™ 7500)	Sphere Fluidics	N/A
Polydimethylsiloxane prepolymer	Dow Corning	Cat #1317318
Sodium chloride	Sigma-Aldrich	Cat #S9888
SU8 3025 photoresist	Fischer Scientific	Cat #NC0057282
SU8 developer	Fischer Scientific	Cat #NC9901158
SSC, 20X	Thermo Fischer Scientific	Cat #15557036
T4 DNA ligase	Petersen et al.[20]	N/A
Topoisomerase 1	Keller et al.[23]	N/A
Critical commercial assays		
ATP solution (100 mM)	Thermo Fischer Scientific	Cat #R0441
dNTP set (100 mM each), PCR grade	Thermo Fischer Scientific	Cat #10297-018
Deposited data		
Negative code, NC	This paper	Data S1
Positive code, PC	This paper	Data S2
Oligonucleotides		
DNA oligo	This paper	N/A
Reporter probe	This paper	N/A
TOP1 DNA nanosensor	Stougaard et al.[13]	N/A
EcoRI DNA nanosensor (blue)	Petersen et al.[20]	N/A
EcoRI DNA nanosensor (red)	Petersen et al.[20]	N/A
Detection probe	Stougaard et al.[13]	N/A
Forward primer (qPCR)	This paper	N/A
Reverse primer (qPCR)	This paper	N/A
DNA template (qPCR)	This paper	N/A
Software and algorithms		
CAD software	Autodesk	https://www.autodesk.com/
GraphPad Prism 10.0.3	GraphPad	https://www.graphpad.com/
ImageJ software	National Institutes of Health	https://imagej.en.softonic.com/
LabVIEW 18.0.1	National Instruments	https://www.ni.com/en.html
Python 3.10.9	Python	https://www.python.org/
Other		
EcoRI (10 U/μL)	Thermo Fischer Scientific	Cat #ER0271
EvaGreen® Dye, 20× in Water	Biotium	Cat #31000
Exonuclease I (20 U/μL)	Thermo Fischer Scientific	Cat #EN0581
Exonuclease III (200 U/μL)	Thermo Fischer Scientific	Cat #EN0191

(*Continued on next page*)

Continued

REAGENT or RESOURCE	SOURCE	IDENTIFIER
Phanta Max Super-Fidelity DNA Polymerase	Vazyme	Cat #P505-d1
Phi29 DNA Polymerase (10 U/uL)	Thermo Fischer Scientific	Cat #EP0092
Photomask	MicroCAD Photo-Mask Ltd.	N/A
Hole-puncher (1.0 mm)	Integra LifeSciences	Cat #33-31AA
Tubing (1.06 mm, PFTE)	Cole-Parmer	N/A

EXPERIMENTAL MODEL AND STUDY PARTICIPANT DETAILS

Experiments were conducted using purified enzymes. Human topoisomerase 1 was expressed and purified by transforming the RS190 yeast strain *Saccharomyces cerevisiae* with the expression plasmid pHT143. The EcoRI restriction enzyme, obtained from Thermo Fischer Scientific, was sourced from E. *coli* containing the cloned *ecoRIR* gene from *Escherichia coli* RY13.

METHOD DETAILS

DNA oligonucleotides

Human TOP1 DNA nanosensor was synthesised by Integrated DNA Technology (Hong Kong SAR). DNA oligo, EcoRI DNA nanosensors (blue and red), reporter probes, and detection probes were purchased from BGI Genomics (Hong Kong SAR). Sequences were listed as the following, where the lower cases mark the preferred human TOP1 recognition sequence and restriction sites of EcoRI:

DNA oligo

5'-/Acr/CCA ACC AAC CAA CCA AAT AAG CGA TCT TCA CAG T-3'. *Reporter probe*: 5'-/FAM/ACT GTG AAG ATC GCT TAT TTG GTT GGT TGG TTG G-3'. *TOP1 DNA nanosensor*: 5′-aga aaa att ttt aaa aaa CTG TGA AGA TCG CTT A ttt ttt aaa aat ttt tct aag tct ttt aga tc CCT CAA TGC ACA TGT TTG GCT CC gat cta aaa gac tta ga-3'. *EcoRI DNA nanosensor (blue; contains primer binding site)*: 5′-/AmC6/ATT CAC T gaattc AGC GCT TAG GAG TGC ATA TAC GAT GCA CTG TGA AGA TCG CTT ATG CAT CGT ATA TGC ACT CCT AAG CGC T gaattc AGT GAA T/AmC6/-3′. *EcoRI DNA nanosensor (red; contains detection probe binding site)*: 5′-/AmC6/ATT TGA C gaattc GTC GTA TAG GAA CTT CGA ACG ACT CGC CTC AAT GCA CAT GTG GCT CCC GAG TCG TTC GAA GTT CCT ATA CGA C gaattc GTC AAA T/AmC6/-3′. *Detection probe*: 5'-/FAM/CCT CAA TGC ACA TGT TTG GCT CC-3'. Specificity of the TOP1 sensor design has previously been demonstrated using various TOP1 enzymes of different origins.[14,15,43] EcoRI sensor specificity was verified by cross-reactivity assessment against similar restriction endonucleases.[20] *Forward primer (qPCR):* 5′-TCG TCG GCA GCG TCA GA-3'. *Reverse primer (qPCR):* 5′-GCC TAC CGC CCA TTT GC-3'. *DNA template (qPCR):* 5′-TCG TCG GCA GCG TCA GAT GTG TAT AAG AGA CAG (N_{12}) GCA AAT GGG CGG TAG GC-3'.

Microfluidic chip designs and fabrication

The microfluidic devices were fabricated using standard soft photolithography process.[44] The patterns were designed by a CAD software (Autodesk, USA) and printed on a photomask (MicroCAD Photo-Mask Ltd., China). According to the manufacturer's instructions, the printed patterns were transferred onto a silicon wafer spin-coated using an SU8 3025 photoresist (Kayaku Advanced Materials, Fischer Scientific, USA). Following exposure, development, and post-exposure bake, the uncrosslinked photoresist was removed by the SU8 developer (Kayaku Advanced Materials, Fischer Scientific, USA). The prepared SU8 molds were measured approximately 25 μm and 50 μm in channel heights for the droplet generation device and the flow microchannel, respectively. Polydimethylsiloxane (PDMS) prepolymer was prepared using the base and curing agent in a 10:1 ratio (w/w) (Dow Corning, USA). The fully mixed mixture was poured onto the SU8 mold and cured overnight at 65°C. Crosslinked PDMS was peeled off from the SU8 mold and cut into slabs. Fluidic inlets and outlets were generated by a hole-puncher of 1.0 mm in diameter (Integra LifeSciences, USA). The PDMS slabs were thoroughly cleaned with ethanol and bonded onto a piece of cover glass through a layer of semi-cured PDMS (a base and curing agent at a weight ratio of 2:1). The bonded assembly was baked at 65°C overnight to further strengthen the bonding.

Fabrication of oligo-conjugated polyacrylamide beads

A polymer mix was prepared in an aqueous solution containing 1% (w/v) ammonium persulfate (Sigma-Aldrich, USA), 10% acrylamide, and bis-acrylamide solution (29:1) (Bio-Rad, USA) and 15 μM 5′acrydite DNA oligo. The solution was loaded into a 1-mL syringe. The oil solution containing 0.5% Pico-Surf (Sphere Fluidics, UK) in HFE-7500 3M Novec (Fluorochem, UK) was loaded into another 1-mL syringe. The two syringes were connected to the oil and aqueous inlets of the droplet generation device (Figure S8A) by 1.06 mm tubing (Cole-Parmer, UK). The flow rate of the aqueous solution and the oil solution were set at 2 μL/min and 8 μL/min, respectively. The droplets were collected from the outlet connected to a collection tube and covered with a layer of mineral oil. Droplets were left for the polymerization overnight at 22°C. The oligo-PAA beads were then released by adding the droplet

destabilizing agent, 1H,1H,2H,2H-perfluoro-1-octanol (final concentration 33% v/v, Sigma-Aldrich, USA), to the emulsion phase. The functionalized oligo-PAA beads were retrieved after eight consecutive washes in 1 mL H_2O and stored at 4°C.

Hydrogel bead-based isothermal detection (BEAD-ID)

The human TOP1 reaction was carried out in a 10 μL reaction volume containing a standard 1× TOP1 reaction buffer (5 mM $CaCl_2$, 5 mM $MgCl_2$, 10 mM Tris-HCl pH 7.5) supplemented with 0.1 μM TOP1 DNA nanosensor. Addition of titrated amounts of purified human TOP1 enzyme (in-house purified, Aarhus University, Denmark) initiated the circularization reaction, producing the TOP1 circular products. The reaction was carried out at 37°C for 2 h and halted by moving the reaction tube −20°C.

The EcoRI endonuclease cleavage was carried out similarly as by Petersen et al.[20] 1 μM of each EcoRI DNA nanosensor was mixed in a 1× EcoRI buffer (Thermo Fischer Scientific, USA). Cleavage of the DNA nanosensors was initiated by addition of titrated EcoRI enzyme (Thermo Fischer Scientific, USA). The reaction was carried out at 37°C for 2 h followed by heat inactivation at 65°C for 20 min. Ligation of the nick was performed by the addition of 10 unit/μL of T4 DNA ligase (in-house purified, Aarhus University, Denmark) and 0.25 mM ATP (Thermo Fischer Scientific, USA) for 60 min at 16°C followed by inactivation of the ligase at 95°C for 10 min. Non-circular products were removed by incubating with 2 units of both exonuclease I and III (Thermo Fischer Scientific, USA) for 1 h at 37°C. Exonuclease digestion was inactivated for 10 min at 95°C. The produced EcoRI circular products were cooled on ice and moved to −20°C.

Oligo-PAA beads were soaked in either 1× TOP1 reaction buffer or 1× EcoRI buffer for 20 min at 22°C depending on the hybridization with human TOP1 or EcoRI circular products, respectively. The beads pellet was spun down at 500 × g for 1 min and the excess liquid was discarded and beads desiccated by vacuum. TOP1 or EcoRI circular products were supplemented with NaCl (Sigma-Aldrich, USA), reaching a final concentration of 250 mM and 300 mM, respectively, prior to their addition to the tube containing desiccated oligo-PAA beads. The ratio employed involved a fixed quantity of oligo-PAA beads, with the number of circular products varying depending on the available enzyme amount during the enzymatic reaction of the nanosensors. Hybridization of the circular products to the oligo-PAA beads was performed for 3 h at 37°C followed by three consecutive washes in 1× Phi29 buffer (Thermo Fischer Scientific, USA). The washed beads were centrifuged at 500 × g for 1 min to remove the supernatant. RCA of the circular products hybridized onto the oligo-PAA beads was performed at 37°C for 2 h in a solution containing 1× Phi29 buffer supplemented with 0.5 μg/μL BSA, 625 μM dNTP (Thermo Fischer Scientific, USA), and 0.5 U/μL Phi29 DNA polymerase (Thermo Fischer Scientific, USA). The RCA reaction was stopped by washing the beads three times in 1× PBS (Gibco, Thermo Fischer Scientific, USA). The excess liquid was removed in between the washes by centrifugation at 500 × g for 1 min. Fluorescence detection was achieved through hybridization of 0.2 μM FAM detection probes in a hybridization buffer containing 20% formamide (Thermo Fischer Scientific, USA), 2× SSC (Thermo Fischer Scientific, USA), and 5% glycerol (Beyotime Biotechnology, China) for 1 h at 37°C followed by three consecutive washes in 1× PBS for 5 min.

Hybridization of reporter probes to oligo-PAA beads and microscopic observations

Titrated concentrations of 5′FAM labelled reporter probes (960, 480, 240, 120, 60, and 0 amol per bead) were incubated with the oligo-PAA beads for 1 h at 37°C under 300 mM NaCl. Following five consecutive washes in 1× PBS pH 7.4, the beads were visualized by fluorescence microscopy (THUNDER Imager Live Cell & 3D Assay, Leica Microsystems, Germany). Fluorescent images were acquired with LED excitation at 475 nm and emission filtering at 535 nm, utilizing an exposure time of 200 ms. Ten z stack images were taken across a total thickness of 25 μm for every field of view. CTBF, as defined in Equation 1,[41] was used as a measure of fluorescent intensities on-bead for the microscopic observation:

$$\text{CTBF} = \text{Integrated Fluorescent Density} - (\text{Area of Selected Bead} \times \text{Mean Fluorescence of Background}), \quad \text{(Equation 1)}$$

where the integrated fluorescent density was obtained by integrating the fluorescent intensities obtained from the z stack. The reported CTBF for every replicate was averaged from at least 10 beads.

QUANTIFICATION OF OLIGOS IN OLIGO-PAA BEADS

A standard quantitative PCR (qPCR) reaction was performed using 1× Phanta Buffer (Vazyme, China), supplemented with 0.2 mM dNTPs, 0.2 μM forward primer, 0.2 μM reverse primer, 0.02 U/μL Phanta Max Super-Fidelity DNA polymerase (Vazyme, China), 1× EvaGreen (Biotium, USA), and either 3% (v/v) oligo-PAA beads or 10% (v/v) DNA template. The oligo-PAA beads (N_{beads}) were varied at 30, 60, 120, 240, 480, or 960 per sample. The DNA template concentrations ranged from 0.01 to 10 nM. The thermocycling conditions included an initial inactivation step at 95°C for 3 min, followed by 25 amplification cycles consisting of denaturation at 98°C for 15 s, annealing at 62°C for 20 s, and extension at 72°C for 20 s. To calculate the number of oligos conjugated in each oligo-PAA bead, the following Equation 2 was used:

$$\text{Oligos per oligo} - \text{PAA bead} = \frac{2^{(x_2 - x_1)} \cdot n_{template} \cdot N_A}{N_{beads}} \quad \text{(Equation 2)}$$

where x_1 and x_2 are the critical values of oligo-PAA beads and template obtained from qPCR, respectively; $n_{template}$ is the number of moles of template used; N_A is Avogrado's constant; and N_{beads} is the total number of oligo-PAA beads in the reaction.

Setup of the microfluidic flow setup

Schematic representation of the microfluidic flow setup is shown in Figure 6A. A blue diode laser emitting at 488 nm (MDL-III-488L/1∼50mW, Changchun New Industries, China) was directed to an inverted fluorescence microscope (Eclipse Ts2R, Nikon, Japan) and used as the excitation source. A 20× objective (NA = 0.95, Nikon, Japan) was used to focus the laser beam pointing to the sample within the microfluidic flow channel (see Figure S8B). The emitted fluorescence from the hydrogel beads was collected through the same objective, passed through a pinhole, and separated from the excitation laser by the dichroic mirror before going through a 30:70 beam splitter. 70% of the light was passed to the high-speed camera (pco.dimax CS3, PCO, Germany) and 30% of the light was passed through a 500–550 nm bandpass filter to a photomultiplier tube (PMT, PMM02-1, Thorlabs, USA). The fluorescence signal was acquired by a data acquisition board (PCIe-6321, National Instruments, USA) at 1 MSPS and processed using both LabVIEW and Python.

Data processing by LabVIEW and Python

LabVIEW (Version 18.0.1, National Instruments, USA) and Python (Version 3.10.9, USA) were employed for data acquisition and analysis, as shown in Figure S6. The LabVIEW module offered direct control for fluorescence detection, real-time display, and data saving with a graphic user interface (GUI). The controls include the on/off control of the 488 nm laser and digitized control of PMT gain voltage based on the intensity of signals. The acquired raw data underwent multiplication by the PMT gain, resulting in calibrated values. These calibrated values, along with the raw data, were saved in a TDMS file at a user-specified location. For subsequent data processing in Python, the *nptdms* library was utilized to read the TDMS file, followed by baseline calculation and signal analysis. The program was bifurcated into two distinct codes: one for analysing the negative (blank) sample (Negative Code, NC, see Data S1) and the other for the positive samples (Positive Code, PC, see Data S2). Both codes extracted the calibration column and saved it as an array of floating points using the *numpy* library. Firstly, the NC pathway was utilized to extract the noise baseline using the blank sample. This involved computing the mean and standard deviation based on 1,000 data points of the blank sample to establish the threshold for noise peak detection. Further refinement of noise peaks from the blank sample was conducted using ROUT outlier removal (Q = 0.5%)[45] in GraphPad Prism (Version 10.0.3, USA). The highest noise peak identified served as threshold for peak identification within positive samples via the PC pathway. For peak characterization, the *scipy* library was employed. As delineated in Figure 6B, the peak characteristics were defined as follows: the peak height was measured from the mean of the baseline obtained from the noise sample to the apex of the peak, while peak width was determined from the widest part of the peak immediately above the mean of the baseline. Peaks wider than 30 were filtered out as potential noise or faulty readings. The area under the curve (AUC) was computed by trapezoidal integration of the peak from the baseline mean to the apex of the peak. These characteristics were then visualized through histograms using *matplot* library, with peak height serving as the sole fluorescence measurement in this study.

QUANTIFICATION AND STATISTICAL ANALYSIS

Limit-of-detection (LOD) was estimated by the 3σ approach.[42] Here, the LOD is calculated using the mean blank response plus three times the standard deviation of the blank measurements. Data was assessed for normality using a Gaussian fit, either through the Shapiro-Wilk test or by visually inspecting histograms fitted with a Gaussian curve. Statistical analysis of the mean of three or more groups was obtained using non-parametric Kruskal-Wallis test with Dunn's multiple comparison test when data were not characterized as normally distributed. For normally distributed data, one-way ANOVA and Tukey's multiple comparison test were applied with significance levels (p values) indicated in the figure legends, showing **, $p < 0.0021$; ***. $p < 0.0002$; ****, $p < 0.0001$; ns, nonsignificant. Data were plotted using GraphPad Prism (Version 10.0.3, USA) and expressed as mean ± standard deviation, calculated from the mean of three independent experiments, following standardization with the mean of the group containing the highest concentration of reporter probes or enzymes.

The sample size required for the detection of TOP1 activity was estimated by statistical power analysis based on Cohen's effect size (f) (Equation 3),

$$f = \sqrt{\frac{\sum (\mu_i - \mu)}{k \cdot \sigma^2}}, \quad \text{(Equation 3)}$$

where k is the number of groups, μ_i is the group mean, μ is the overall mean, and σ is the standard deviation. The smallest estimated effect size was 0.092. With a desired power level of 80% and a significance level (α) of 0.05, and considering a total of 5 groups, the maximum required sample size was determined to be 1,411.